RSC Advances

PAPER

View Article Online
View Journal | View Issue

Cite this: *RSC Adv.*, 2021, **11**, 15856

Novel construction of carbon nanofiber/$CuCrO_2$ composite for selective determination of 4-nitrophenol in environmental samples and for supercapacitor application†

Subramanian Sakthinathan,*[a] Ramachandran Rajakumaran,[b] Arjunan Karthi Keyan,[a] Chung-Lun Yu,[a] Chia-Fang Wu,[a] Sivaramakrishnan Vinothini,[c] Shen-Ming Chen[b] and Te-Wei Chiu *[a]

A simple hydrothermal process has been used to prepare a carbon nanofiber/copper chromium dioxide (CNF/$CuCrO_2$) composite for the selective detection of 4-nitrophenol (4-NP) and supercapacitor applications. The electrochemical sensor was developed with a glassy carbon electrode (GCE) modified with the CNF/$CuCrO_2$ composite by the drop-casting method. The structural formation of the prepared materials was confirmed by infrared spectroscopy, electrochemical impedance spectroscopy, Raman spectroscopy, scanning electron microscopy, X-ray diffraction, and transmission electron microscopy. To investigate the electrochemical efficiency of the electrode, various electroanalytical techniques, namely, differential pulse voltammetry (DPV), cyclic voltammetry (CV) and galvanostatic charge–discharge tests, were employed. The GCE/CNF/$CuCrO_2$ modified electrode exhibited excellent electrocatalytic behavior for the detection of 4-NP under optimized conditions with a low detection limit (0.022 μM), long linear response range of 0.1–150 μM, and high sensitivity (20.02 μA μM^{-1} cm^{-2}). The modified electrode was used for the detection of 4-NP in real samples with satisfactory results. In addition, the GCE/CNF/$CuCrO_2$ electrode has advantages such as stability, reproducibility, repeatability, reliability, low cost, and practical application. The CNF/$CuCrO_2$ composite coated Ni-foam electrodes also exhibited excellent supercapacitor efficiency, with a high specific capacitance of up to 159 F g^{-1} at a current density of 5 A g^{-1} and outstanding cycling stability. Hence, the CNF/$CuCrO_2$ composite is a suitable material for 4-NP sensors and energy storage applications.

Received 9th April 2021
Accepted 20th April 2021

DOI: 10.1039/d1ra02783b

rsc.li/rsc-advances

1. Introduction

The accurate detection of nitroaromatic compounds such as nitrotoluene, nitrobenzene, and nitrophenol in natural water sources is important for environmental safety because they result from a broad range of activities.[1,2,18] Especially, 4-nitrophenol (4-NP) is extensively used as an intermediate in the production of pesticides, pharmaceuticals, dyestuffs, leather fungicide, analgesics, and acid–base indicators. It can cause serious adverse effects due to its toxicity and persistence, and it is considered a major hazardous pollutant in the environmental ecosystem.[3] It is a bio-refractory organic compound that is anthropogenic, acidic, inhibitory, and toxic. The detoxification of water contaminated with 4-NP is extremely difficult due to its high chemical stability and resistance to microbial degradation.[3,4] Moreover, 4-NP can enter the environment during its production and application in industry and agriculture.[5] It is toxic to plants, sea animals, and mammals, even in very low concentrations, due to its high solubility and low degradability.[5,18] For these reasons, 4-NP has been included in environmental legislation because it is a teratogen and carcinogen, and it induces mutagenic activity in humans.[6,7,42] For example, 4-NP is one of the top classified environmental toxins in the United States Environmental Protection Agency (USEPA) due to its persistence and toxicity.[8,9] Moreover, brief exposure to inhalation of 4-NP can induce headaches, fatigue, vomiting, and cyanosis in humans. In addition, 4-NP is considered a dangerous food cycle pollutant that appears to remain in grains, fruits, vegetables, or water supplies when it is a component of fertilizers or pesticides.[10–12] Therefore, the preparation

[a]*Department of Materials and Mineral Resources Engineering, National Taipei University of Technology, No. 1, Section 3, Chung-Hsiao East Road, Taipei 106, Taiwan. E-mail: sakthinathan1988@gmail.com; tewei@ntut.edu.tw*

[b]*Department of Chemical Engineering and Biotechnology, National Taipei University of Technology, No. 1, Section 3, Chung-Hsiao East Road, Taipei 106, Taiwan*

[c]*Department of Computer Science and Information Engineering, National Taipei University of Technology, No. 1, Section 3, Chung-Hsiao East Road, Taipei 106, Taiwan*

† Electronic supplementary information (ESI) available: Real sample analysis and comparison of the specific capacitance values of different oxide systems. See DOI: 10.1039/d1ra02783b

of a quickly responsive, selective, and low-cost technique for the identification of 4-NP in environmental samples for food safety and environmental safety is essential.[13]

During the last few years, numerous analysis methods have been used for the identification of 4-NP, some examples being gas chromatography, spectrofluorometry, capillary zone electrophoresis, spectrophotometry, enzyme-linked immunosorbent assay, and high-performance liquid chromatography.[14–16] However, these above-mentioned methods require expensive apparatus, long analysis times, and tedious sample pretreatment.[17] As a result, there is high demand for a cost-effective detection method for 4-NP that requires little instrumentation, is easy to operate and rapid, and has high sensitivity and selectivity.[18] Electrochemical detection is considered as a possible approach because of its high sensitivity, simplicity, fast analysis, real-time monitoring, ease of miniaturization, rapidity, and low cost. In addition, electrodes are easy and inexpensive to fabricate, and they have excellent reproducibility and high sensitivity in electrochemical detection.[19] Consequently, the electrode material is the main component for the electrochemical detection of 4-NP.[20] An unmodified GCE shows poor electrocatalytic activity such as sensitivity and selectivity for 4-NP detection. Therefore, chemically modified electrodes are established in 4-NP sensing to resolve the problems of the unmodified electrode. Modification of the working surface of the electrode can boost the efficiency of electrochemical sensors. A broad range of resources, including inorganic, organic, and polymeric molecules, as well as metal nanoparticles, have been used to modify electrodes to enhance selectivity. However, no studies on determination of 4-NP by using an inorganic complex fabricated GCE electrode have been reported to date.[21–23] In recent years, delafossite structured composites have been used extensively for modified electrodes to prepare reliable electrochemical sensors.

Transparent conducting oxides (TCOs) are used in transparent electrodes, flat panel displays, optoelectronic devices, and transparent conducting film. In 1997, Kawazoe *et al.* stated that the ABO_2 structured delafossite oxides are stable p-type broadband transparent semiconductors, where A has a triangular pattern and BO_2 is an octahedral flattened structure.[24,25] In addition, Cu delafossite compounds ($Cu_IM_{III}O_2$ (M = Co, In, B, Al, Cr, Ga)) have been used in electronic applications due to their low-lying valence band, simple preparation and high hole mobility.

In particular, $CuCrO_2$ has properties suitable for p-type TCO, such as high optical transparency because of its direct optical bandgap (3.3 eV) and low valence band edge.[26] In p-type $CuCrO_2$, the Cu vacancy is an internal predominant defect, so holes notably exist in the Cu 3d-orbital. Therefore, $CuCrO_2$ materials can be considered as sensor electrode materials of outstanding quality with low working potential.[27,28] However, $CuCrO_2$ has some limits in sensor applications due to its low stability and the limited surface area of the electrode surface. To reduce these limits, different approaches or modifications (covalent or non-covalent) of $CuCrO_2$ with other stable carbon materials have been used to increase the electrocatalytic properties of $CuCrO_2$.[29,30]

In materials science, carbon nanofibers (CNF) have received notable attention for the application in electroanalysis, electrochemical capacitors, dye-sensitized solar cells, Li-ion batteries, transparent conducting electrodes, nanodevices, and antimicrobial agents.[31,32] In addition, CNF are biocompatible, and they have a large surface area (448 $m^2\ g^{-1}$), excellent electrical conductivity, and chemical and thermal stability. In addition, CNF have cylindrical structures with graphene sheet stacking configurations such as herringbone, platelet stacking, and ribbon. The diameter sizes of CNF vary from a few tens of nanometers to many hundreds of nanometers.[33] CNF have more edges on the outer wall, which may facilitate the higher electron transfer properties, and the whole surface area can be activated electrochemically without damage to the structural integrity.[34,35] Therefore, CNF are suitable for use as an electrode material with $CuCrO_2$ in electrochemical sensors because of the specific properties described above.[36]

Renewable and alternative energy sources have become a great challenge due to the enormous global consumption of energy and climate change. In various energy storage systems, batteries and electrochemical capacitors play major roles in electrical energy storage.[37] Supercapacitors are a special class of energy storage devices with high voltage, long cycle life, and high-power capacity, as well as good stability, higher specific capacitance rates, high power densities, fast charge–discharge rates, and high coulombic efficiency.[38] They are used in a variety of practical applications, such as electronic devices, electric vehicles, and other storage systems for renewable energy. Supercapacitors not only retain energy but also release stored energy within a short period. The essential elements of a high-performance supercapacitor are maximum power density, fast charge–discharge, and high stability.[39] Supercapacitors can be divided into two classifications, namely, electric double-layer capacitors (EDLCs) and pseudocapacitors, depending on the efficiency of energy storage. In addition, pseudocapacitors and EDLCs have a low specific capacitance for redox reactions, electrosorption, and intercalation processes. As a pseudocapacitor electrode for enhancing capacitance, many materials with high surface areas and redox activity have been used. For example, CNTs, graphene, carbon nanofibers, transition metal oxides, and conductive polymers have exhibited good performance for supercapacitor electrode preparation.[40,41]

Metal oxide nanocomposites are widely used as a significant component for improving the selectivity and sensitivity of working electrodes in electrochemical methods. In addition, metal oxides are notable for their simplicity and ease of fabrication, sensitivity, wide surface area, and high catalytic activity.[42] In the present study, a sensor electrode was modified with CNF/$CuCrO_2$ composite prepared by hydrothermal methods. The $CuCrO_2$ was evenly distributed on the surface of the CNF due to the non-covalent interaction between the CNF and $CuCrO_2$ to form a new type of nanocomposite for 4-NP detection and supercapacitor applications. As CNF have easily accessible surface areas, this property was used to immobilize the $CuCrO_2$ complexes on the electrode surface and increase the electron transfer on the surface of the electrode. The GCE/CNF/$CuCrO_2$ electrode demonstrated excellent electrochemical

efficiency with a low detection limit, fast response, excellent reproducibility, and simplicity for the detection of 4-NP. In addition, the highly active CNF/$CuCrO_2$ composite coated Ni foil electrode showed a higher specific capacitance and excellent cycling stability during the supercapacitor performance. From these studies, we found that the CNF/$CuCrO_2$ composite has excellent bifunctional activity for electroanalytical and capacitance performance.

2. Materials and methods

Chromium nitrate, copper nitrate, carbon nanofiber, glycine, sodium acetate, ethanol, acetic acid, hydrochloric acid, polyvinylidene difluoride, *N*-methyl pyrrolidinone, potassium hydroxide, sulfuric acid, sodium phosphate dibasic, and dihydrogen sodium phosphate were purchased from Sigma Aldrich, Taiwan. The dihydrogen sodium phosphate (NaH_2PO_4) and disodium hydrogen phosphate (Na_2HPO_4) were used for preparing the phosphate buffer solution (PBS). The CNF/$CuCrO_2$ composite was studied by different physicochemical characterization techniques. The phase structure was identified by X-ray diffraction (XRD, D2 Phaser, Bruker) with CuKα radiation (λ = 1.540 Å). High-resolution transmission electron microscopy (HR-TEM) and field emission scanning electron microscopy were used for the surface morphology analysis.

A scanning transmission electron microscope (STEM, JEM-2100F) with energy dispersive X-ray (EDS) spectrum analysis validated the elemental distribution. The electrochemical sensor performance of the GCE/CNF/$CuCrO_2$ modified electrode was studied by cyclic voltammetry (CV) and differential pulse voltammetry (DPV). All the electrochemical experiments were measured using a CHI 210 electrochemical workstation (CH Instruments Co., Austin, TX, USA). For voltammetry tests, a three-electrode device, with Ag/AgCl electrode as a reference electrode, GCE as the working electrode, and platinum wire as an auxiliary electrode, was used. All the electrochemical studies were performed at room temperature, and the pH was determined by Suntex pH meter (SP-2100).

2.1 Preparation of GCE/CNF/$CuCrO_2$ electrode

Chromium nitrate, copper nitrate, and glycine were used as starting reagents for the preparation of $CuCrO_2$. The glycine to metal nitrate molar ratio was set at 1.5. To obtain transparent solutions, the necessary quantities of copper nitrate (2416 g), chromium nitrate (4 g), and glycine (1125 g) were dissolved in distilled water. After stirring at 80 °C for 2 h, the obtained solution was heated to 100 °C and dried for 24 h to obtain a transparent substance. This transparent glass material was then heated to about 300 °C in a beaker and spontaneously ignited to yield a gray $CuCrO_2$ powder mass.[25,26]

First, the obtained $CuCrO_2$ and CNF (mass ratio of 4 : 1) were placed in 15 mL of deionized water. Then a few drops of NaOH (0.5 mol) solution were added and the solution was stirred until the pH reached 10. The obtained material was poured into a Teflon-lined autoclave (20 mL) and heated for 12 h at 180 °C before being cooled to laboratory temperature. These acquired products were gathered many times with ethanol and water. After that, the collected materials were dried at 80 °C for 10 h to obtain the composite of CNF/$CuCrO_2$.

2.2 Preparation of the GCE/CNF/$CuCrO_2$ electrode for the 4-NP sensor

To fabricate the electrode, bare GCE was polished with alumina slurry (0.05 μm) with a polishing kit until a mirror-like surface emerged. After that, the polished bare GCE was gently washed

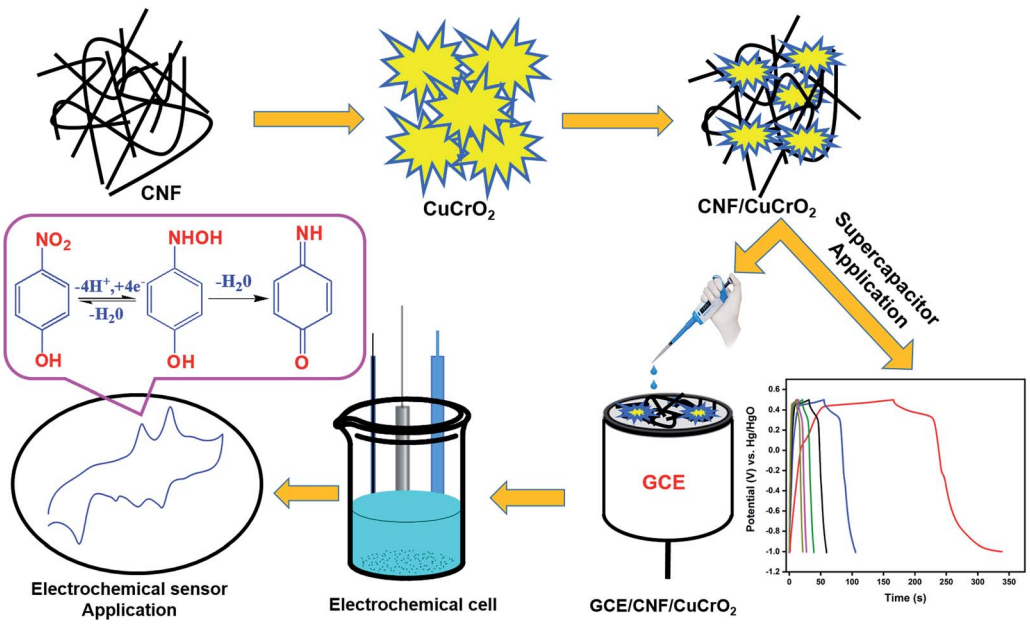

Scheme 1 Preparation of GCE/CNF/$CuCrO_2$ electrode for detection of 4-NP and supercapacitor.

and dried with ethanol and distilled water at room temperature. In addition, the CNF/$CuCrO_2$ (5 mg) composite was dispersed in 1 mL of water–methanol solution by ultrasonic irradiation for 20 minutes to obtain a homogenous CNF/$CuCrO_2$ suspension. After that, 8 μL of the prepared CNF/$CuCrO_2$ composite solution was drop-cast on the pre-cleaned GCE electrode. The prepared GCE/CNF/$CuCrO_2$ electrode was dried and applied for 4-NP sensor studies (Scheme 1).

2.3 Supercapacitor electrode preparation

The supercapacitor working electrode was prepared as follows. The synthesized CNF/$CuCrO_2$ composite material, graphite, and the binder polyvinylidene difluoride (PVDF) were combined with *N*-methyl pyrrolidinone to form slurry. After that, 20 μL of the prepared slurry was coated by the drop-casting method on the 1 × 1 cm^2 area of the Ni foil electrode and dried for 6 h at 60 °C. The mass loading level of the CNF/$CuCrO_2$ composite on the Ni foil was 1 mg cm^{-2}.

Before the electrochemical analysis, the prepared Ni foam electrode was submersed in a 1.0 M KOH electrolyte solution for a few hours. Finally, in a three-electrode cell system with a potential range of 0–1.5 V and 1.0 M KOH aqueous electrolyte solution, the electrochemical behavior of the electrodes was investigated. Ni foam-coated CNF/$CuCrO_2$ materials were used as the working electrode, Ag/AgCl as the reference electrode, and platinum (Pt) wire as the counter electrode. The electrochemical properties of the electrodes were studied by cyclic voltammetry (CV) and galvanostatic charge–discharge (GCD) methods.

3. Results and discussion

3.1 Characterization of the prepared materials

Fig. 1 shows the XRD patterns of pristine (A) CNF, (B) $CuCrO_2$, and (C) CNF/$CuCrO_2$ composites. The XRD spectrum of CNF exhibited a broad diffraction peak at $2\theta = 25.3°$, which corresponds to the (002) plane of amorphous natural hexagonal graphitic carbon. The reflection spectra of $CuCrO_2$ nanoparticles were obtained at the 2θ values of 30.42, 35.21, 35.45, 41.88, 48.85, 54.92, 61.38, 66.62, 72.54, and 73.49, corresponding to the (006), (101), (012), (104), (009), (018), (110), (0012), (116), and (202) planes of the hexagonal crystal structure of $CuCrO_2$ (JCPDS no: 740983). This was in concordance with previously reported $CuCrO_2$ diffraction results. The XRD pattern of the CNF/$CuCrO_2$ composite presented reflections corresponding to the CNF and $CuCrO_2$ crystalline phase, in good agreement with the SEM studies. The CNF/$CuCrO_2$ composite peaks confirmed that the pure $CuCrO_2$ was adsorbed on the CNF surface to form CNF/$CuCrO_2$ composite.

The surface morphologies of the CNF, $CuCrO_2$, and CNF/$CuCrO_2$ were characterized by SEM and TEM studies. Fig. 2A shows that the one-dimensional CNF had a tube-like structure with an average diameter of 200 nm. In addition, the CNF had a wide surface area and accelerated electron transfer properties due to rough surfaces and more defects. Fig. 2B shows a SEM image of the $CuCrO_2$ particles, which were spherical with uniform size distribution and irregular shape arrangements. Fig. 2C and 2D present SEM images of CNF/$CuCrO_2$ composite showing the surface of the CNF covered with $CuCrO_2$ complex. The CNF/$CuCrO_2$ composite consisted of a CNF core and

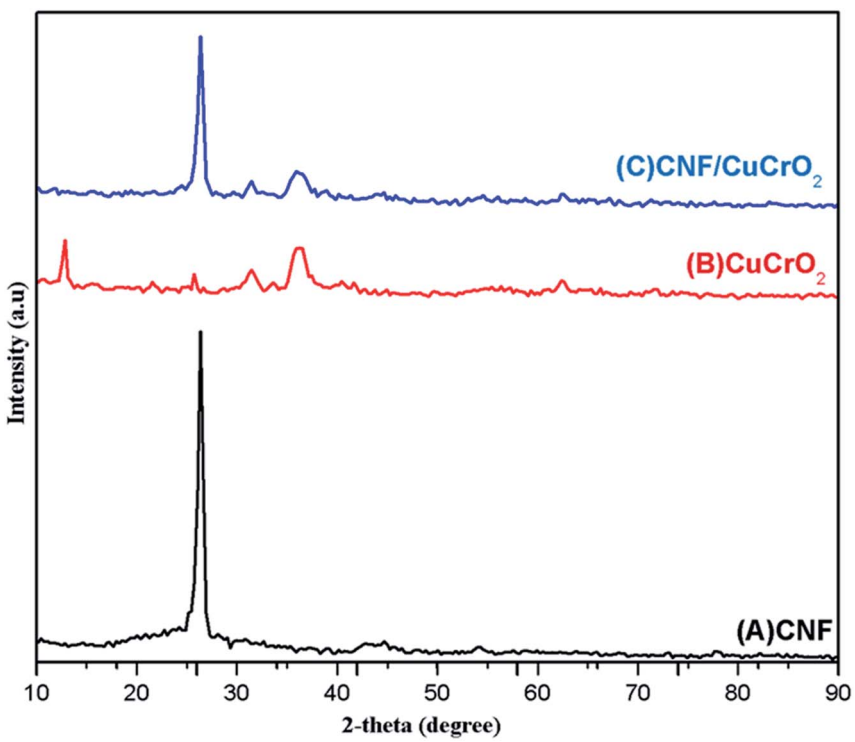

Fig. 1 XRD spectra of (A) CNF, (B) $CuCrO_2$, and (C) CNF/$CuCrO_2$ powder.

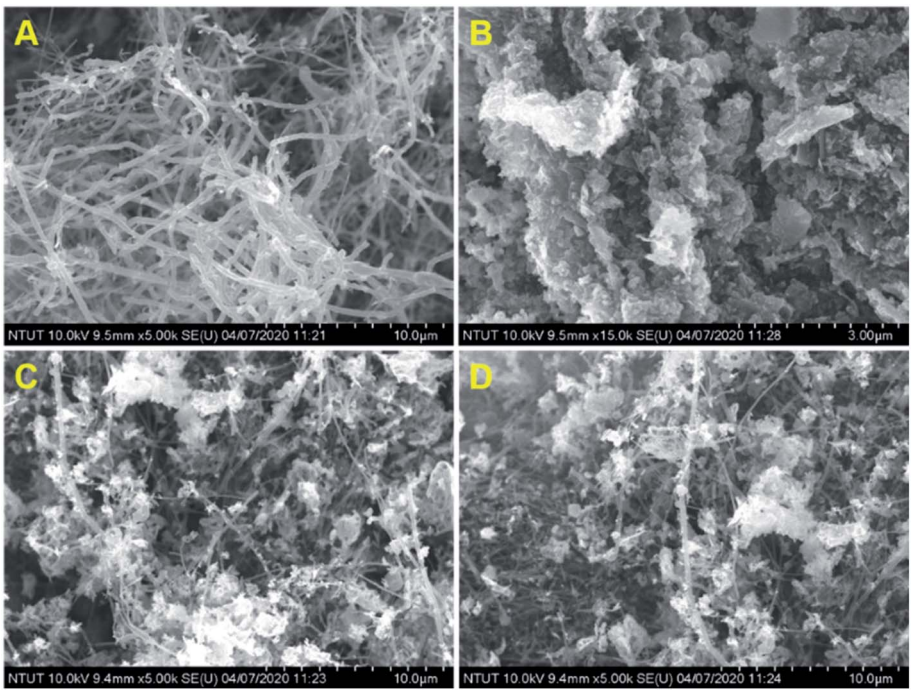

Fig. 2 SEM image of (A) CNF, (B) $CuCrO_2$, (C and D) CNF/$CuCrO_2$.

a $CuCrO_2$ shell with a grooved structure. The CNF/$CuCrO_2$ composite had a hierarchically porous interconnected structure with a large inner surface area. Fig. 3 shows the elemental mapping spectra of the CNF/$CuCrO_2$ composite. The results showed that the (C) Cu, (D) Cr, (E) C, and (F) O elements were homogeneously distributed on the CNF/$CuCrO_2$ composite surface. Fig. 4 shows TEM images of (A) CNF, (B) $CuCrO_2$, and (C) CNF/$CuCrO_2$ composite. The structure of the CNF was

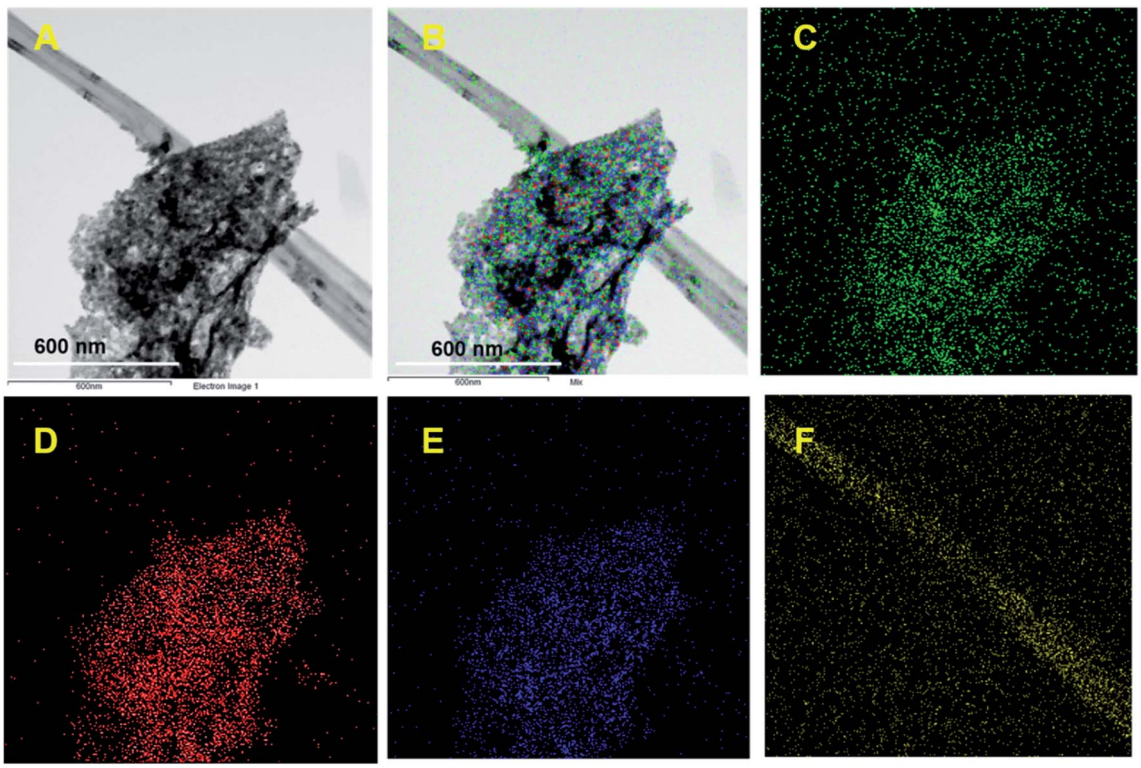

Fig. 3 (A) and (B) Elemental mapping of CNF/$CuCrO_2$ shows (C) Cu, (D) Cr, (E) C, and (F) O.

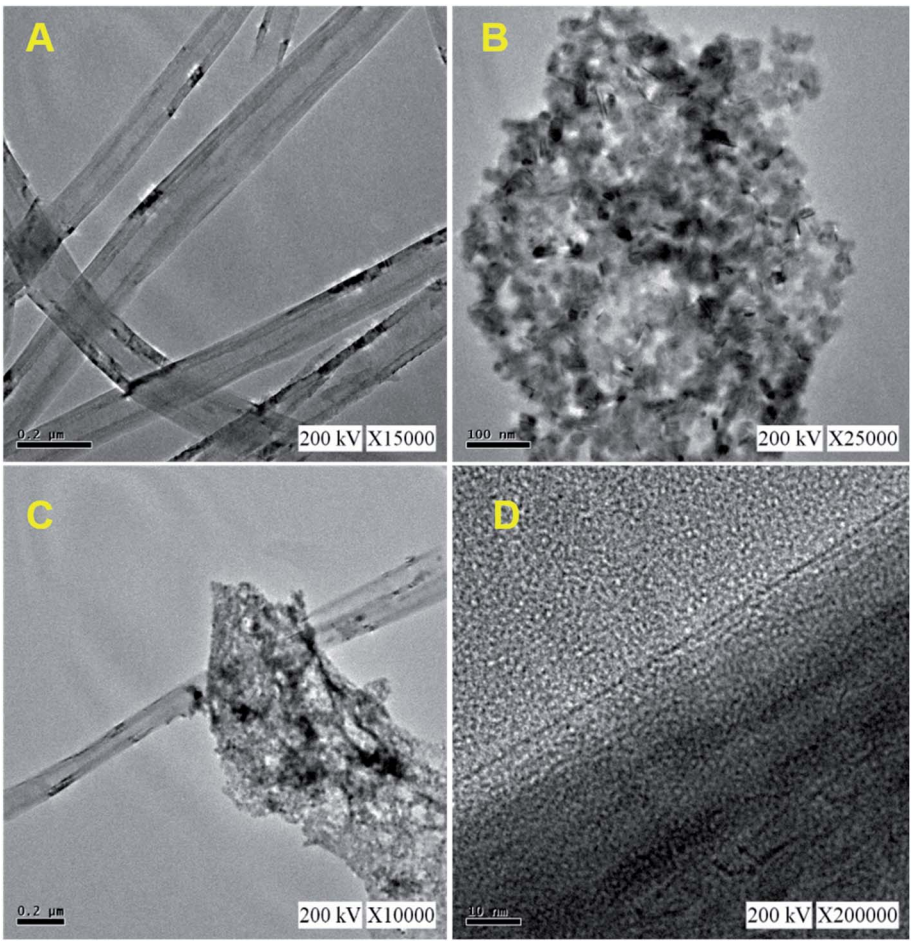

Fig. 4 TEM images of (A) CNF, (B) $CuCrO_2$, and (C and D) CNF/$CuCrO_2$ composite.

multiple hollow tubular structures with an oriented smooth surface. The TEM images of the $CuCrO_2$ complex showed aggregated small cubes and a randomly arranged structure. Also, the TEM image of the CNF/$CuCrO_2$ composite revealed that the $CuCrO_2$ was incorporated onto the CNF surface, providing more active sites for electrochemical reaction.

Fig. 5A shows the FT-IR spectra of (a) CNF, (b) $CuCrO_2$, (c) CNF/$CuCrO_2$. The CNF exhibited broad bands at 1200 cm^{-1} and 1540 cm^{-1} owing to the C–C stretching vibration and COO– symmetric stretching vibration, respectively. The peak at around 2858 cm^{-1} was ascribed to $-CH_2-$ stretching vibration and 3422 cm^{-1} ascribed to –OH stretching vibration. Moreover, the FT-IR spectrum of the $CuCrO_2$ complex exhibited a weak band at 939 cm^{-1} and strong bands at 742 cm^{-1} and 536 cm^{-1} for the Cr^{III}–O and M–O stretching frequencies. Finally, the spectrum of CNF/$CuCrO_2$ exhibited the vibrational bands of $CuCrO_2$, confirming the successful incorporation of the copper complex on the CNF.

Raman spectroscopy was used to identify the formation of carbon-based materials. Fig. 5B presents the Raman spectra of the (a) CNF, (b) $CuCrO_2$, and (c) CNF/$CuCrO_2$ material. In the Raman spectra of CNF, D band at 1364 cm^{-1} and the G band at 1584 cm^{-1} suggested that the graphitic band. The D band was attributed to the disordered (sp^2 site) existence of the graphite formation, and the G band, to the C–C stretching of the graphite material. The Raman spectra of prepared $CuCrO_2$ consisted of two modes at 452 cm^{-1} and 703 cm^{-1} for E_g and A_g^1 and some weak modes found at 208 cm^{-1} and 536 cm^{-1} due to Cu vacancies. The Raman spectra for CNF/$CuCrO_2$ composite showed peak around 1345 cm^{-1} and 1580 cm^{-1} for the bare CNF and $CuCrO_2$ samples.

The precise binding state and the chemical composition arrangement of the as-prepared CNF/$CuCrO_2$ composite were studied by XPS analysis. The obtained wide scan survey spectrum of the as-prepared CNF/$CuCrO_2$ composite is presented in Fig. 6A. All the elements, namely, Cu, Cr, C, and O, were observed in the wide scan spectrum, revealing the successful formation of the $CuCrO_2$/CNF composite. Fig. 6B shows the high-resolution spectra of Cu 2p. The two main peaks were Cu $2p_{1/2}$ and Cu $2p_{3/2}$ at 960.49 and 940.50 eV, corresponding with the spin-orbital splitting energy of about $\Delta_{Cu\ 2p} = 19.9$ eV, in good accordance with the reported data of the $CuCrO_2$ phase.[30,43,44] These observed results indicated that Cu existed in the +1 oxidation state. In addition to that, the Cu spectrum exhibited two satellite peaks at 950.24 and 942.95 eV, corresponding to the +2 oxidation ionic state of Cu $2p_{1/2}$ and Cu $2p_{3/}$

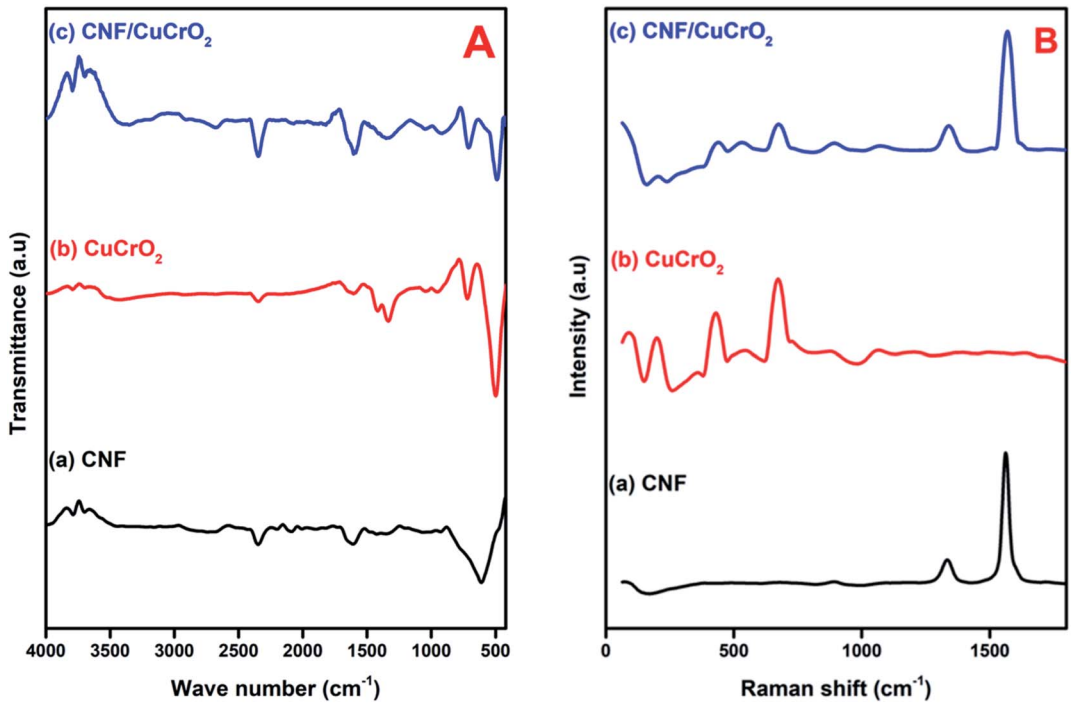

Fig. 5 (A) FT-IR spectra of (a) CNF, (b) $CuCrO_2$, (c) CNF/$CuCrO_2$ composite. (B) Raman spectra of (a) CNF, (b) $CuCrO_2$, (c) CNF/$CuCrO_2$ composite.

$_2$. These results suggested that the Cu retained both +1 and +2 oxidation states in the prepared $CuCrO_2$/CNF catalyst. The binding energies of Cr indexed at 584.29 and 577.44 eV are attributed to the ionic state of +3 in the prepared $CuCrO_2$/CNF catalyst (Fig. 6C). Furthermore, the incorporation of CNF into the $CuCrO_2$ showed the presence of a C 1s peak with its consisting binding energies at 292.92 and 284.85 eV (Fig. 6D). The C 1s peaks illustrated the combination of C–C bands at 285.85 eV and the carboxyl carbon peak (O–C=O) observed at 292.92 eV. Fig. 6E presents the O 1s spectrum. It can be deconvoluted into two peaks separated at binding energies of 540.45 and 539.18 eV and belonging to the oxygen vacancy surface defects and adsorbed oxygen forming single-bonded carbon (C–O).[4,5] Finally, the XPS studies confirmed the formation of the CNF/$CuCrO_2$ composite.

EIS is an important electroanalytical technique, and it has widespread applications in research for analyzing various phenomena, namely electrode-material interfacial resistance, charge transfer kinetics, mass transfer property, and diffusion coefficients. It is also used to characterize and monitor electrical conductivity and the sensitivity of an electrochemical system. The electrochemical activity of the prepared catalyst was checked in 5 mM $[Fe(CN)_6]^{3-/4-}$. The Nyquist plot was obtained from a frequency spectrum of 100 mHz to 100 kHz in 0.1 M KCl solution, and the obtained results for different prepared electrodes are shown in Fig. 7A. The plot generally comprises two regions, namely, a semicircular zone and a linear zone. The semicircular zone, at a higher amplitude region, is ascribed to the charge transfer resistance (R_{ct}), while the linear zone, at a lower frequency region, is attributed to the diffusion process. From the obtained results, it was observed that the bare GCE exhibited a higher R_{ct} value of about 303 Ω, indicating a poor electron transfer process at the bare GCE. The $CuCrO_2$ fabricated on the GCE showed lower resistance than that of the bare GCE, and the R_{ct} value notably decreased to 166 Ω, due to its excellent catalytic property. With the surface modification of GCE with CNF, the resistance was lower because it had a high basic surface area, which could enable the direct electron kinetics reaction process with good electrical conductivity. The R_{ct} value was about 92 Ω. The GCE/CNF/$CuCrO_2$ electrode delivered a very low R_{ct} value of 65 Ω due to the synergistic effect of $CuCrO_2$ and CNF. The findings clearly illustrate that the GCE/CNF/$CuCrO_2$ exhibited an excellent electrocatalytic kinetics process, and the R_{ct} value was much lower than those of other electrodes. The R_{ct} values of bare GCE, GCE/$CuCrO_2$, GCE/CNF, and GCE/CNF/$CuCrO_2$ electrodes are compared in Fig. 7B.

3.2 Electrochemical performance of 4-nitrophenol at modified electrodes

The electrochemical studies of 4-NP by different electrodes were analyzed by the CV method. Fig. 8A displays the CV response from the unmodified GCE, GCE/CNF, GCE/$CuCrO_2$, and GCE/CNF/$CuCrO_2$ in the presence of 4-NP in N_2 purged PBS at pH 5.0. Without the addition of 4-NP in 0.5 M PBS, there was no electrochemical response in this potential range. The results for all the aforementioned electrodes in response to the redox reaction of 4-NP are listed in Table 1. With the bare GCE, the redox peaks for 4-NP were very small, at about 0.2 V. The intensities of the redox peaks increased steadily for the GCE modified with CNF, $CuCrO_2$, and CNF/$CuCrO_2$ composites. The electrocatalytic

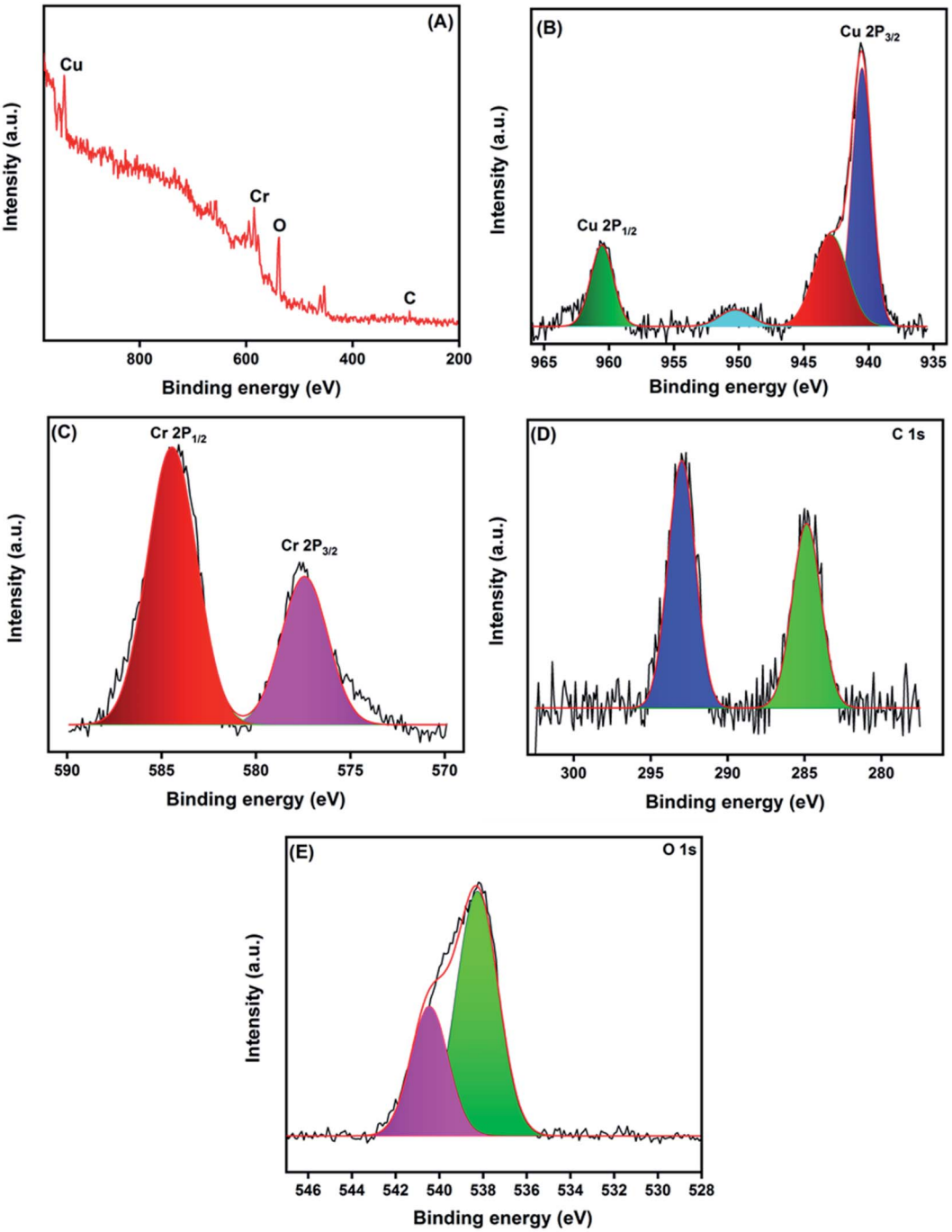

Fig. 6 XPS survey spectrum of CNF/$CuCrO_2$ composite (A), core level spectrum of Cu 2p (B), Cr 2p (C), C 1s (D), and O 1s (E).

response of CNF/$CuCrO_2$ to 4-NP was higher than those of bare GCE, CNF, and $CuCrO_2$. The GCE/CNF/$CuCrO_2$ electrode exhibited a high peak current for 4-NP reduction due to the high surface area and good electron transfer properties (Fig. 8B). Moreover, the synergistic effect of CNF and $CuCrO_2$ made the GCE/CNF/$CuCrO_2$ composite exhibit the highest electrocatalytic activity for 4-NP detection.

The electrochemical activity of GCE/CNF/$CuCrO_2$ 4-NP is shown in Fig. 8B. The figure shows a pair of main 4-NP oxidation/reduction (redox) peaks (O_1/R_1) at around 0.2 V. Moreover, 4-NP exhibits two pairs of weak oxidation/reduction peaks (O_2/R_2 and O_3/R_3) at 0.4 and 0.6 V and two reduction peaks (R) at 0.4 and 0.6 V. The reversible two-electron redox reaction of 4-aminophenol is shown by the three pairs of redox (oxidation/reduction) peaks (O_1/R_1, O_2/R_2, and O_3/R_3). To create the hydroxylamine species, the two R peaks exhibit an irreversible reduction of the nitro group. The possible electrocatalytic reactions of 4-NP on the GCE/CNF/$CuCrO_2$ electrode are described in Scheme 2. The overall electrochemical redox activity of 4-NP is very close to that of previously recorded

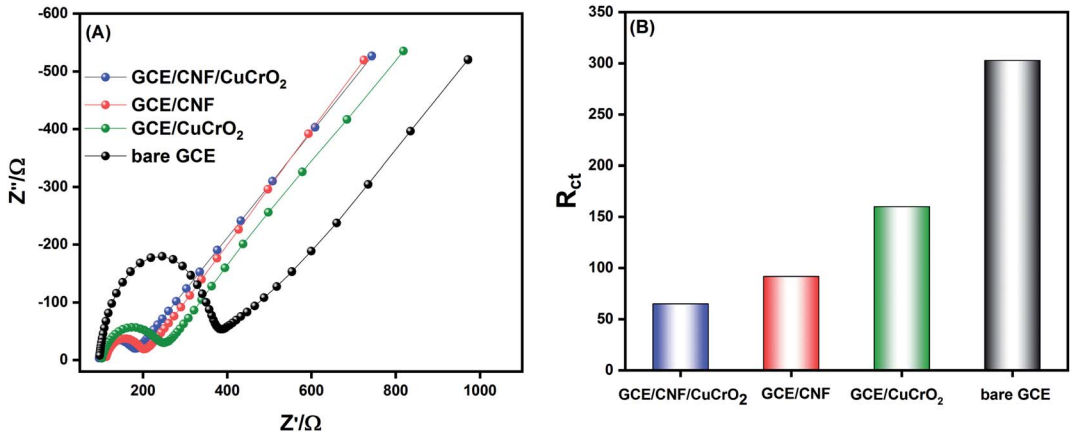

Fig. 7 (A) EIS studies of (a) bare GCE, (b) GCE/CNF, (c) GCE/$CuCrO_2$, and (d) GCE/CNF/$CuCrO_2$ modified electrodes in 0.1 M KCl at 5 mM $[Fe(CN)_6]^{3-/4-}$. (B) R_{ct} values of bare GCE, GCE/$CuCrO_2$, GCE/CNF, and GCE/CNF/$CuCrO_2$ electrodes.

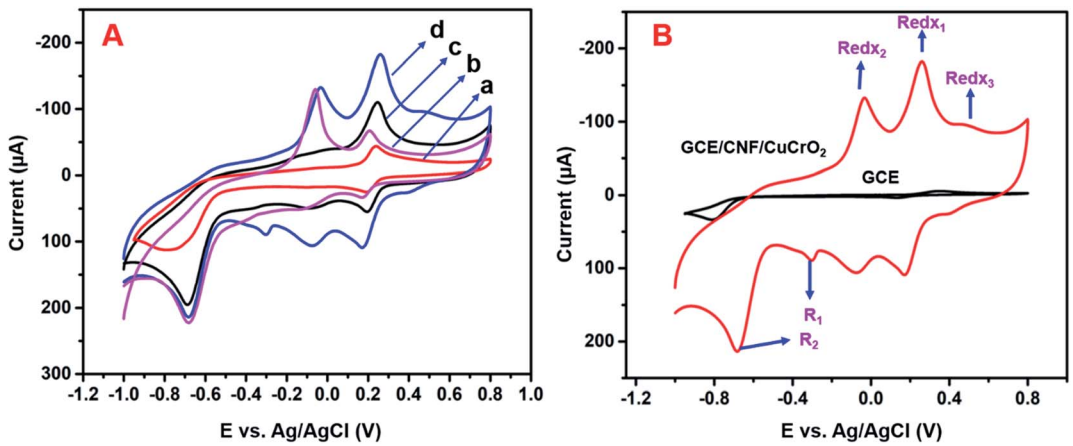

Fig. 8 (A) CV studies of (a) bare GCE, (b) GCE/CNF, (c) GCE/$CuCrO_2$, and (d) GCE/CNF/$CuCrO_2$ electrodes in the presence of 1.0 μM of 4-NP in PBS (pH = 5.0) at a scan rate of 50 mV s^{-1} and (B) CV response of (a) GCE/CNF/$CuCrO_2$ and (b) bare GCE in the presence of 4-NP in PBS (pH = 5.0).

Table 1 Comparison of electrochemical detection performance of GCE/CNF/$CuCrO_2$ electrode with other modified electrodes

Electrode materials	Linear range (μM)	Detection limit (μM)	Ref.
GCE/CNF/$CuCrO_2$	0.1–150	0.022	This work
Nafion/Mb-HAp@CNF/CILE	0.3–10.0	0.23	36
GO/GCE	0.1–120	0.02	1
OMCs/GCE	2.0–90	0.1	24
f-MWCNTs/ZrO_2/GCE	2–26	0.03	9
Silver particles/GCE	1.5–140	0.5	44
AgA-PE	0.2–100	0.3	45
DTD/Ag NP/CPE	1–100	0.25	46
ERG/AuNP/GCE	0.036–90	10	47
Kao/IL/PdNP/GCE	0.5–4.5	22	48
PCZ/NGE/GCE	0.8–20	62	49
AgNW@PANI/GCE	0.6–32	52	50
SWCNT/GCE	0.01–5.0	2.5	6
CeO_2–Cu_2O	—	2.85	51
CeO_2–Cu_2O/CH	—	2.03	51

work.[45–51] Fig. 9A shows that the electrochemical performance of GCE/CNF/$CuCrO_2$ improved when the concentration of 4-NP was increased, and the corresponding linear range was from 0.1 to 200 μM. Fig. 9B presents the corresponding linear relation between the concentration of 4-NP and the peak current (I_p) for the 4-NP oxidation.

3.3 Effects of different pH on 4-NP detection

Electrolyte pH conditions can strongly influence the electrochemical detection of 4-NP. The influence of pH was investigated using CV studies. The peak current and potential of the 4-NP were close to the pH value of the electrolyte solution. Fig. 10A presents the electrochemical detection of 4-NP over the GCE/CNF/$CuCrO_2$ electrode under various pH conditions. It can be seen that, when the pH increased from 3 to 5, the redox peak current equally increased, while at pH 5 to 9, the peak potential changed to the negative side and the peak current decreased. The highest redox peak current appeared at pH 5, so we used pH 5 for further electrochemical studies. The high redox response

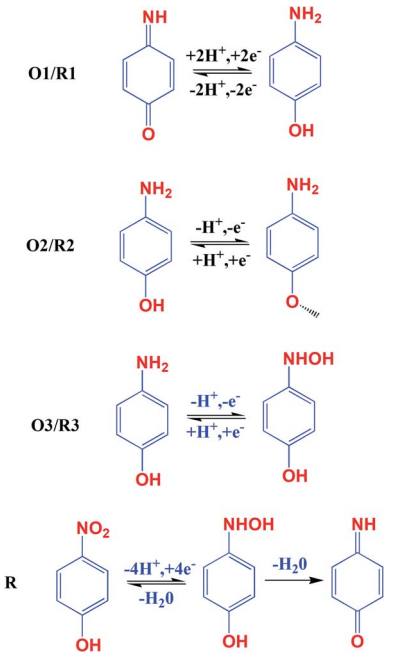

Scheme 2 Electrocatalytic mechanisms of 4-NP over the GCE/CNF/$CuCrO_2$ electrode.

at pH 5 might have been related to the strong interaction between the negatively charged GCE/CNF/$CuCrO_2$ electrode surface and the positively charged nitrophenol species (protonated). Furthermore, an acidic environment is more favorable for the redox reaction of 4-NP, in agreement with the proposed reactions in Scheme 2.[4,6,7]. The linear regression equation can be revealed as E_{pa} (V) = −0.057 pH + 0.557 (R^2 = 0.989), which is given below:

$$E_p = -(0.0592m/n)\ \text{pH} + b$$

According to the Nernst equation, the ratio of m/n was identified as 1.42, where m is the number of proton transfers, T is temperature, n is the electron transfer number, R is the gas constant (8.314 J K^{-1} mol^{-1}), and F is the Faraday constant (96 485.33 C mol^{-1}). Based on the Nernst equation, an equal number of electrons and protons were involved at the time of 4-NP detection over the GCE/CNF/$CuCrO_2$ electrode. Moreover, Fig. 10B indicates that the maximum peak current response to pH was a pK_a value of 4-NP, which determined that the non-dissociated 4-NP was adsorbed more over the GCE/CNF/$CuCrO_2$ electrode. The linear relation between pH and peak current potential is shown in Fig. 10C. A slope of 57 mV pH^{-1} for the electrochemical reaction indicates an equal number of electron transfers with the GCE/CNF/$CuCrO_2$ electrode.

3.4 Effect of different scan rates

The electrocatalytic mechanism is generally obtained from the relation between the scan rate and peak current. The consequence of the scan rate on the reduction of 4-NP at the GCE/CNF/$CuCrO_2$ electrode was also investigated in 0.05 M PBS containing 200 μM 4-NP at scan rates of 10–500 mV s^{-1}. Fig. 11A shows that the redox peak currents linearly increased as the scan rate increased. In addition, the redox potential moved to the positive and negative sides as the scan rate rose. Fig. 11B presents the plot of redox peak current *vs.* square root of scan rate. The corresponding linear regression equation can be revealed as eqn (3): $I_p = -36.752\nu^{1/2} + 117.2$ (R^2 = 0.9955). This result indicates that the detection process of 4-NP over the GCE/CNF/$CuCrO_2$ electrode is diffusion-controlled. These results reveal that the GCE/CNF/$CuCrO_2$ electrode has outstanding electrochemical properties due to its high porosity and excellent electrocatalytic function. Furthermore, the high surface area of the GCE/CNF/$CuCrO_2$ electrode creates fast electron transfers between the electrode and 4-NP.

3.5 Determination of 4-NP by DPV studies

DPV is a more responsive method than other cyclic voltammetric systems. Hence, we conducted DPV studies for determining the sensitivity, linearity, and detection limit of the modified electrode. Fig. 12A depicts the DPV responses of 4-NP reduction on GCE/CNF/$CuCrO_2$ in 0.05 M PBS with different

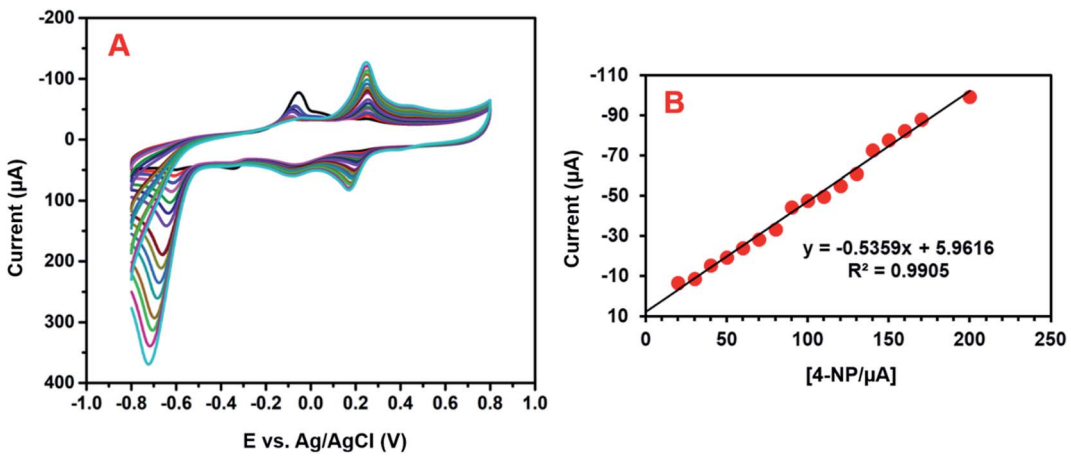

Fig. 9 (A) The obtained CV response for the GCE/CNF/$CuCrO_2$ electrode for the detection of 0.1 to 200 μM 4-NP in PBS. (B) Calibration plot between the peak current and concentration of 4-NP.

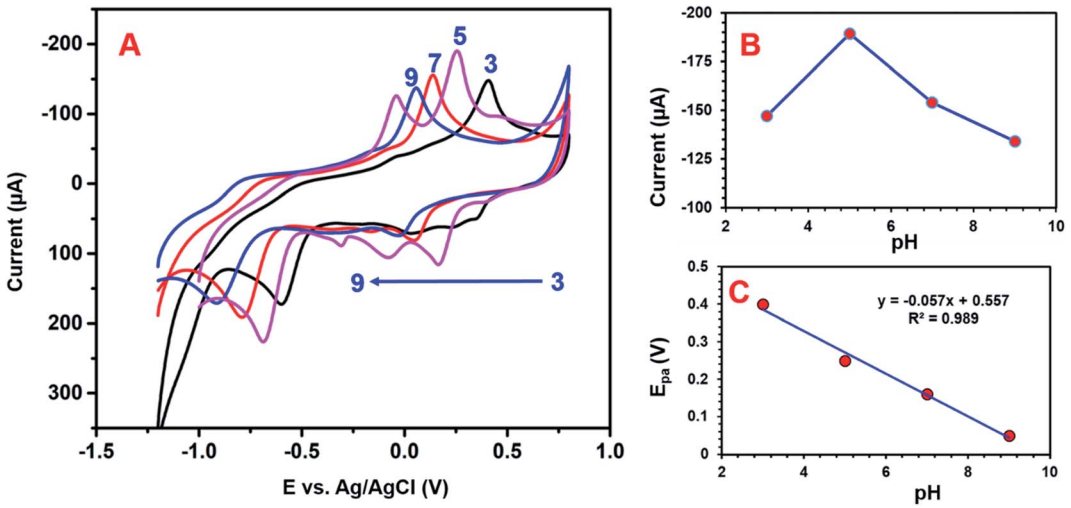

Fig. 10 (A) Cyclic voltammogram of GCE/CNF/$CuCrO_2$ electrode under deoxygenated conditions at pH 3 to pH 9. (B) The inset shows the pH values *versus* peak current. (C) The inset shows the pH values *versus* oxidation peak potential.

concentrations of 4-NP (0.1–150 μM). The reduction peak current rose with increases in the concentration of 4-NP. Fig. 12B reveals that the linear concentration range of the modified electrode was 0.1–150 μM and the detection limit (LOD) was 0.022 μM. Moreover, the sensitivity of the GCE/CNF/$CuCrO_2$ electrode was 20.02 μA μM^{-1} cm^{-2}, which was greater than those of other 4-NP sensors. The obtained results are compared with those of the reported 4-NP sensors in Table 1. The GCE/CNF/$CuCrO_2$ electrode presents better results for the identification of 4-NP due to the greater electron transfer rate and good catalytic properties of $CuCrO_2$. Furthermore, the high surface area of CNF allows for close interaction between the CNF and $CuCrO_2$. Therefore, the GCE/CNF/$CuCrO_2$ electrode is a superb electrode material for the electrochemical identification of 4-NP.

3.6 Repeatability, reproducibility and stability studies

The selectivity behavior of the GCE/CNF/$CuCrO_2$ electrode was studied with the DPV system in the presence of 20 μM 4-NP in acetate PBS solution along with interference molecules and ions, namely, (a) Zn^{2+}, (b) Co^{2+}, (c) Ni^{2+}, (d) Na^+, (e) Mg^{2+}, (f) Ca^{2+}, (g) K^+, and (h) NO_3^-. The 4-NP response showed no loss, even in the presence of interfering metal ion species (Fig. 13A). The results strongly indicate that the GCE/CNF/$CuCrO_2$ electrode is suitable for selective detection of 4-NP. Moreover, the operational stability of the electrode was examined by a CV technique in the presence of 100 μM 4-NP. The experimental performance showed a 4-NP peak current loss of only 2.3% from the initial current (Fig. 13B). The obtained results indicate good operational stability. Moreover, storage stability is understood to be a main factor in electrochemical sensor studies. The storage stability of the GCE/CNF/$CuCrO_2$ electrode was examined periodically in 100 μM of PBS containing 4-NP. After 15 days of storage, the GCE/CNF/$CuCrO_2$ electrode showed a peak current change of 3.3% from its initial peak response. The reproducibility and repeatability of the GCE/CNF/$CuCrO_2$ electrode were examined by cyclic voltammetry in PBS including 0.1 mM 4-NP. The GCE/CNF/$CuCrO_2$ electrode demonstrated reasonable reproducibility of 2.74% in 10 independent studies with 10 independent electrodes (Fig. 13C). The prepared

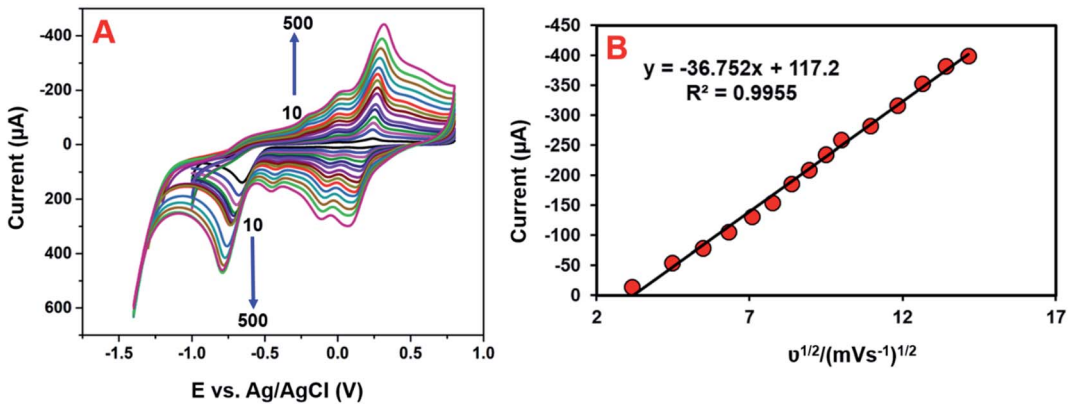

Fig. 11 (A) CV curves of GCE/CNF/$CuCrO_2$ electrode in the presence of 1.0 μM 4-NP in 0.05 M PBS (pH 5.0) were observed at various scan rates of 10–500 mV s^{-1}. (B) Correlations between the peak currents and the square root of the scan rate.

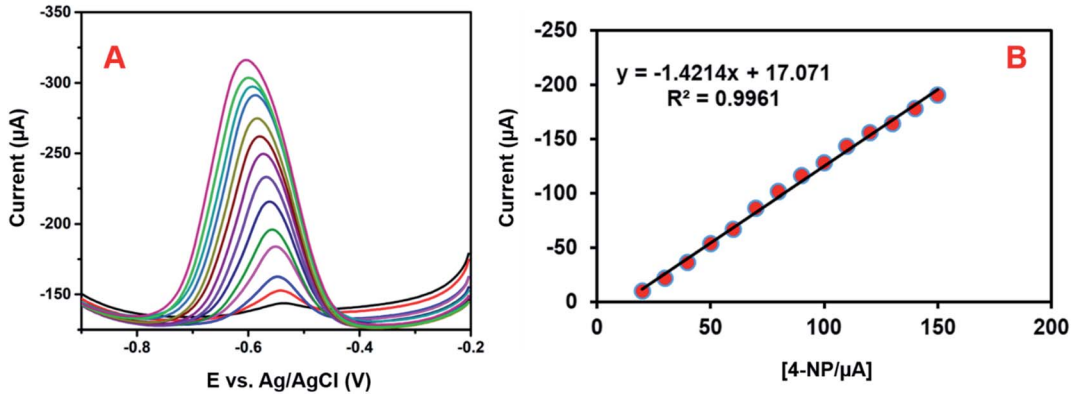

Fig. 12 (A) DPV performance of GCE/CNF/$CuCrO_2$ electrode in 4-NP solution at different concentrations. (B) Plot of peak current *versus* concentration of 4-NP.

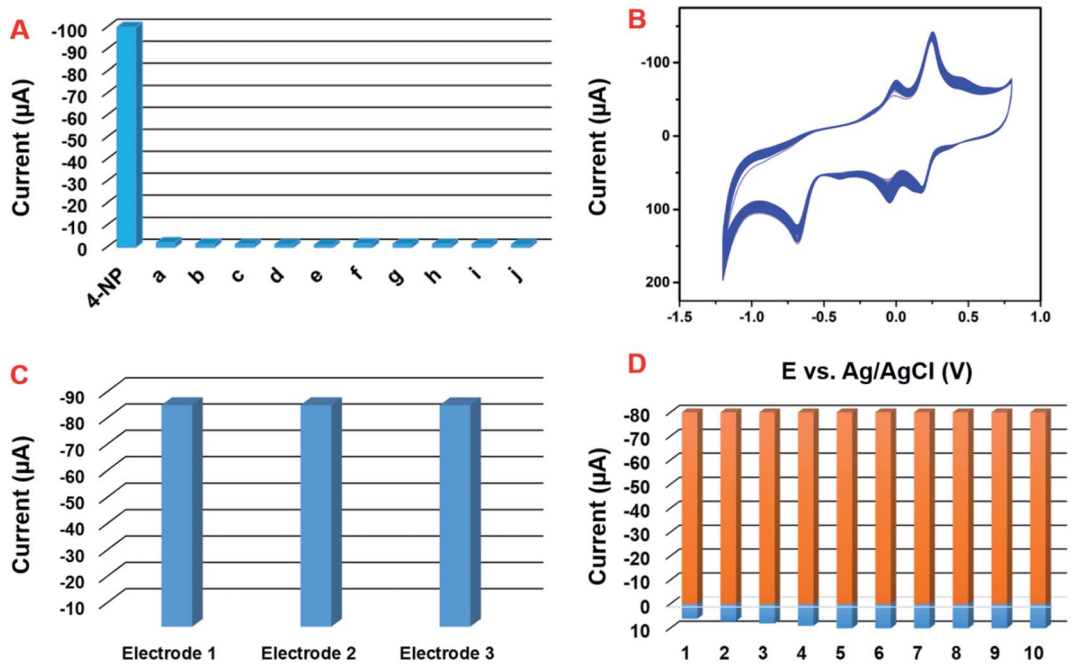

Fig. 13 (A) Bar diagram for interference analysis of GCE/CNF/$CuCrO_2$ electrode by CV in 0.05 M PBS. (B) The stability test of the GCE/CNF/$CuCrO_2$ electrode in the presence of 100 μM 4-NP in N_2 purged 0.05 M PBS (pH 5.0) at a scan rate of 50 mV s^{-1} for 10 successive measurements. (C) The reproducibility of the GCE/CNF/$CuCrO_2$ electrode for three different electrodes. (D) The repeatability of the GCE/CNF/$CuCrO_2$ electrode with the same electrode.

electrodes presented an acceptable percentage of current performance, 2.32% for 10 repeated measurements conducted with a single GCE/CNF/$CuCrO_2$ electrode (Fig. 13D). These studies provide further evidence that the GCE/CNF/$CuCrO_2$ electrode has excellent repeatability and reproducibility. All these aforementioned studies indicate that the GCE/CNF/$CuCrO_2$ electrode has excellent repeatability, reproducibility, and stability.

3.7 Real sample analysis

The practical ability of the prepared electrode to detect 4-NP was examined by the CV method using tap water, industrial waste water and river water, and the obtained CV results are given in S. Fig. 1A–C. The tap water samples were collected from our laboratory and the river water samples were collected from the Yonghe River in Taipei. The industrial waste water was collected from nearby factory in Taipei. The collected samples were used for real sample analysis with the GCE/CNF/$CuCrO_2$ modified electrode. Before the real sample identification, the collected water samples were centrifuged at 2000 rpm to remove contaminants and the pH was adjusted to 5.0. After that, the real sample studies showed no 4-NP signal unless 4-NP was added, indicating that the 4-NP concentration was lower than the detection limit. For this reason, the conventional standard

Table 2 Determination of 4-NP in different water samples by GCE/CNF/$CuCrO_2$ electrode

Samples	Added (μM)	Found (μM)	Recovery (%)	(RSD) (%)
Tap water	10	9.8	98	3.2
	10	19.9	99.5	2.7
River water	10	9.3	93	3.5
	10	19.5	97.5	3.7
Industrial waste water	10	9.5	95	3.2
	10	19.7	98.5	2.8

addition approach was used for the recovery of the actual real sample analysis, and the results are listed in Table 2. In the real sample experiment, the GCE/CNF/$CuCrO_2$ electrode exhibited an admissible recovery percentage of 95–99.5%. Therefore, these results exhibit that the GCE/CNF/$CuCrO_2$ electrode is reliable and has potential for the detection of 4-NP in real samples.

4. Electrochemical performance

The CNF/$CuCrO_2$ composite with nickel foam (NF) was used as a supercapacitor electrode. The electrochemical behavior of the prepared CNF/NF, $CuCrO_2$/NF, CNF/$CuCrO_2$/NF electrodes was determined by the cyclic voltammetry (CV) technique and the galvanostatic charge–discharge (GCD) measurement of the standard three-electrode cell system in 1 M KOH liquid electrolyte. Fig. 14A displays the CV profiles of the CNF/NF, $CuCrO_2$/NF, and CNF/$CuCrO_2$/NF electrodes at a scan rate of 10 mV s^{-1}. The CV shows that the curve obtained for CNF/$CuCrO_2$/NF electrode was larger than those of the CNF/NF and $CuCrO_2$/NF, indicating better charge storage and stability. In addition, the specific capacitances of CNF/NF, $CuCrO_2$/NF, and CNF/$CuCrO_2$/NF electrodes were determined using CV curves with the following eqn (1).[37,38]

$$C_{sp} = \left(\int i\,dV\right) \Big/ (S \times \Delta V \times m) \quad (1)$$

where m denotes the mass of the electrode active material (mg), S is the scan rate (mV s^{-1}), ΔV is the potential window (V), and $\int i\,dV$ is the integral region of the CV peak. The specific capacitance values for CNF/NF, $CuCrO_2$/NF, and CNF/$CuCrO_2$/NF were 103, 54, and 159 F g^{-1}, respectively. The capacitance values for the CNF/$CuCrO_2$/NF electrode were higher than those for CNF/NF and $CuCrO_2$/NF electrodes due to the high rate of ion exchange on the electrode surface.

Fig. 14B shows the electrochemical behavior of the CNF/$CuCrO_2$/NF electrode at an operating potential range of 0.5–1.0 V at various scan rates (10–50 mV s^{-1}). The CV curves exhibit distinctive redox peaks, suggesting the charge storage mechanism of the CNF/$CuCrO_2$/NF electrodes, which were regulated by a faradaic redox reaction mechanism and thus possessed pseudo-capacitive actions relative to the Cu^{2+}/Cu^{+} pair. Moreover, anodic and cathodic peak separation improved from a lower scanning rate to higher scanning rates for electrode

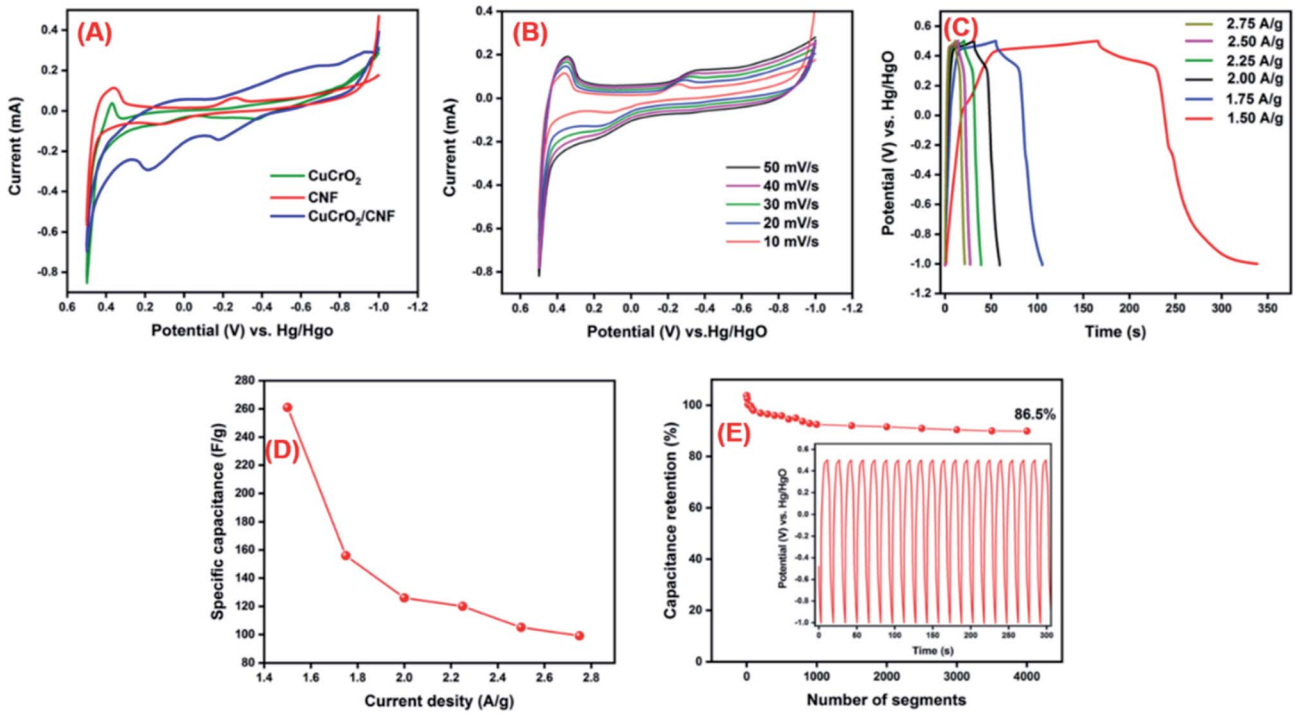

Fig. 14 (A) Electrochemical performance of $CuCrO_2$/NF, CNF/NF, and CNF/$CuCrO_2$/NF electrodes in 1.0 M KOH. (B) The CNF/$CuCrO_2$/NF electrodes with various scan rates (10–50 mV s^{-1}). (C) The GCD curves of CNF/$CuCrO_2$/NF electrodes at various current densities (1.50–2.75 A g^{-1}). (D) Capacitance values for the samples as a function of current density. (E) Cycle stability of CNF/$CuCrO_2$/NF electrodes in 1.0 M KOH at a current density of 5 A g^{-1}. (Inset: potential variation with time during the charge–discharge for first twenty cycles).

polarization and ohmic resistance during redox reactions. The redox peak and shapes of the curves appeared up to the higher scan rate of 50 mV s^{-1} due to improved electron conduction and mass transfer inside the electrode.

GCD studies were used to examine further electrochemical properties of the supercapacitor materials. Fig. 14C presents the GCD studies of CNF/$CuCrO_2$/NF at current densities of 1.50, 1.75, 2.00, 2.25, 2.50, and 2.75. The discharge curves exhibited a pseudocapacitance performance that was compatible with the above-mentioned CV results. The CNF/$CuCrO_2$/NF electrode had average specific capacitances of 261, 156, 126, 120, 105, and 99 A g^{-1} at those current densities, respectively. As shown in Fig. 14D, the obtained real capacitance of the present CNF/$CuCrO_2$/NF electrode was very comparable to those of several reported electrodes. From these studies, the specific capacitance of the CNF/$CuCrO_2$/NF electrode is reduced with increasing current density.[39,46]

In addition, stability is one of the main requirements for supercapacitor fabrication. Fig. 14D presents the cycle stability of the CNF/$CuCrO_2$/NF composite electrode, which was explored by repeated GCD between −1.0 and 0.5 V over 4000 segments at a current density of 5 A g^{-1}. The specific capacitance measured for certain intermittent cycles is plotted against the corresponding cycles (Fig. 1D inset). The specific capacitance of the CNF/$CuCrO_2$/NF electrode decreased by 13.5%, and about 86.5% capacitance remained. The CNF/$CuCrO_2$/NF electrode showed excellent stability and high precise capacitance due to the inclusion of CNF and $CuCrO_2$. Therefore, the capacitance performance of the CNF/$CuCrO_2$/NF electrode was higher than those of previously recorded materials, as shown in S. Table 1. Based on the aforesaid electrochemical studies, the prepared CNF/$CuCrO_2$/NF compound has remarkable potential for use as an electrode material in supercapacitor devices.

5. Conclusions

In conclusion, we have successfully prepared a CNF/$CuCrO_2$ composite *via* hydrothermal methods. The prepared composite was characterized by X-ray diffraction, scanning transmission electron microscopy, CHI cyclic voltammetry studies, and scanning electron microscopy. The GCE/CNF/$CuCrO_2$ modified electrode exhibits a high peak current response for the detection of 4-NP due to its high electrochemical activity. The GCE/CNF/$CuCrO_2$ electrode shows excellent performance in the reduction of 4-NP because of the π–π interaction between the electrode materials and 4-NP. Furthermore, the linear response range of 4-NP was found to be 0.1–150 μM, the sensitivity was 20.02 μA μM^{-1} cm^{-2}, and the detection limit was 0.022 μM. The real sample studies of the GCE/CNF/$CuCrO_2$ electrode in water samples produced acceptable detection levels. The GCE/CNF/$CuCrO_2$ electrode has outstanding selectivity, stability, sensitivity, and reproducibility for the detection of 4-NP. At a current density of 5 A g^{-1}, the CNF/$CuCrO_2$/NF composite coated Ni foam electrode has a high specific capacitance of 159 F g^{-1} with an excellent electron transfer rate capability and cyclability. Therefore, the GCE/CNF/$CuCrO_2$ electrode presented herein can be used for the identification of 4-NP and for energy storage application.

Conflicts of interest

The authors declare no competing financial interest.

Acknowledgements

The Ministry of Science and Technology of Taiwan supported this work (MOST 109-2221-E-027-059 and 109-2222-E-027-001). The author is grateful to the Precision Research and Analysis Center of the National Taipei University of Technology (NTUT) for providing the measurement facilities.

References

1 J. Li, D. Kuang, Y. Feng, F. Zhang, Z. Xu and M. Liu, *J. Hazard. Mater.*, 2012, **201–202**, 250–259.
2 M. Ramalingam, V. K. Ponnusamy and S. N. Sangilimuthu, *Environ. Sci. Pollut. Res.*, 2020, **27**, 17481–17491.
3 S. B. Khan, K. Akhtar, E. M. Bakhsh and A. M. Asiri, *Appl. Surf. Sci.*, 2019, **492**, 726–735.
4 R. Madhu, C. Karuppiah, S. M. Chen, P. Veerakumar and S. Bin Liu, *Anal. Methods*, 2014, **6**, 5274–5280.
5 P. Wang, J. Xiao, M. Guo, Y. Xia, Z. Li, X. Jiang and W. Huang, *J. Electrochem. Soc.*, 2015, **162**, H72–H78.
6 C. Yang, *Microchim. Acta*, 2004, **148**, 87–92.
7 Y. Tang, R. Huang, C. Liu, S. Yang, Z. Lu and S. Luo, *Anal. Methods*, 2013, **5**, 5508–5514.
8 Y. Cheng, Y. Li, D. Li, B. Zhang, R. Hao and S. Sang, *Int. J. Electrochem. Sci.*, 2017, **12**, 7754–7764.
9 B. Devadas, M. Rajkumar, S. M. Chen and P. C. Yeh, *Anal. Methods*, 2014, **6**, 4686–4691.
10 S. B. Khan, K. Akhtar, E. M. Bakhsh and A. M. Asiri, *Appl. Surf. Sci.*, 2019, **492**, 726–735.
11 A. Liao, P. Li, H. Zhang, M. Guo, Y. Xia, Z. Li and W. Huang, *J. Electrochem. Soc.*, 2017, **164**, H63–H69.
12 I. Tapsoba, S. Bourhis, T. Feng and M. Pontié, *Electroanalysis*, 2009, **21**, 1167–1176.
13 M. Govindhan, T. Lafleur, B. R. Adhikari and A. Chen, *Electroanalysis*, 2015, **27**, 902–909.
14 F. Jalali, A. T. AbdAli and Z. Hasanvand, *Adv. Environ. Sci. Technol.*, 2018, **4**, 51–60.
15 A. Arvinte, M. Mahosenaho, M. Pinteala, A. M. Sesay and V. Virtanen, *Microchim. Acta*, 2011, **174**, 337–343.
16 L. qiang Luo, X. lian Zou, Y. ping Ding and Q. sheng Wu, *Sens. Actuators, B*, 2008, **135**, 61–65.
17 D. Hofmann, F. Hartmann and H. Herrmann, *Anal. Bioanal. Chem.*, 2008, **391**, 161–169.
18 D. K. Dang, C. Sundaram, Y. L. T. Ngo, W. M. Choi, J. S. Chung, E. J. Kim and S. H. Hur, *Dyes Pigm.*, 2019, **165**, 327–334.
19 M. A. El Mhammedi, M. Achak, M. Bakasse and A. Chtaini, *J. Hazard. Mater.*, 2009, **163**, 323–328.
20 W. Huang, C. Yang and S. Zhang, *Anal. Bioanal. Chem.*, 2003, **375**, 703–707.

21 H. Yin, Y. Zhou, S. Ai, X. Liu, L. Zhu and L. Lu, *Microchim. Acta*, 2010, **169**, 87–92.
22 Y. Zeng, Y. Zhou, T. Zhou and G. Shi, *Electrochim. Acta*, 2014, **130**, 504–511.
23 T. Zhang, Q. Lang, D. Yang, L. Li, L. Zeng, C. Zheng, T. Li, M. Wei and A. Liu, *Electrochim. Acta*, 2013, **106**, 127–134.
24 T. W. Chiu, B. S. Yu, Y. R. Wang, K. Te Chen and Y. Te Lin, *J. Alloys Compd.*, 2011, **509**, 2933–2935.
25 Y. T. Nien, M. R. Hu, T. W. Chiu and J. S. Chu, *Mater. Chem. Phys.*, 2016, **179**, 182–188.
26 T. W. Chiu, Y. C. Yang, A. C. Yeh, Y. P. Wang and Y. W. Feng, *Vacuum*, 2013, **87**, 174–177.
27 R. Manickam, J. Yesuraj and K. Biswas, *Mater. Sci. Semicond. Process.*, 2020, **109**, 104928.
28 S. Zhou, X. Fang, Z. Deng, D. Li, W. Dong, R. Tao, G. Meng and T. Wang, *Sens. Actuators, B*, 2009, **143**, 119–123.
29 A. Varga, G. F. Samu and C. Janáky, *Electrochim. Acta*, 2018, **272**, 22–32.
30 B. Tong, Z. Deng, B. Xu, G. Meng, J. Shao, H. Liu, T. Dai, X. Shan, W. Dong, S. Wang, S. Zhou, R. Tao and X. Fang, *ACS Appl. Mater. Interfaces*, 2018, **10**, 34727–34734.
31 J. Sun, Y. Liu, S. Lv, Z. Huang, L. Cui and T. Wu, *Electroanalysis*, 2016, **28**, 439–444.
32 J. Huang, Y. Liu and T. You, *Anal. Methods*, 2010, **2**, 202–211.
33 Z. Huo, Y. Zhou, Q. Liu, X. He, Y. Liang and M. Xu, *Microchim. Acta*, 2011, **173**, 119–125.
34 Q. Guo, J. Huang, P. Chen, Y. Liu, H. Hou and T. You, *Sens. Actuators, B*, 2012, **163**, 179–185.
35 Y. Yang, R. Fu, J. Yuan, S. Wu, J. Zhang and H. Wang, *Microchim. Acta*, 2015, **182**, 2241–2249.
36 J. Mu, C. Shao, Z. Guo, Z. Zhang, M. Zhang, P. Zhang, B. Chen and Y. Liu, *ACS Appl. Mater. Interfaces*, 2011, **3**, 590–596.
37 H. Cheng and H. M. Duong, *RSC Adv.*, 2015, **5**, 30260–30267.
38 N. Arjun, G. T. Pan and T. C. K. Yang, *Results Phys.*, 2017, **7**, 920–926.
39 V. Veeramani, R. Madhu, S. M. Chen and M. Sivakumar, *ACS Sustainable Chem. Eng.*, 2016, **4**, 5013–5020.
40 V. Veeramani, R. Madhu, S. M. Chen, M. Sivakumar, C. Te Hung, N. Miyamoto and S. Bin Liu, *Electrochim. Acta*, 2017, **247**, 288–295.
41 C. Wang, F. Li, H. Qu, Y. Wang, X. Yi, Y. Qiu, Z. Zou, Y. Luo and B. Yu, *Electrochim. Acta*, 2015, **158**, 35–41.
42 N. I. Ikhsan, P. Rameshkumar and N. M. Huang, *Electrochim. Acta*, 2016, **192**, 392–399.
43 J. Crêpellière, P. L. Popa, N. Bahlawane, R. Leturcq, F. Werner, S. Siebentritt and D. Lenoble, *J. Mater. Chem. C*, 2016, **4**, 4278–4287.
44 J. Liu, W. Weng, H. Xie, G. Luo, G. Li, W. Sun, C. Ruan and X. Wang, *ACS Omega*, 2019, **4**, 15653–15659.
45 I. G. Casella and M. Contursi, *J. Electrochem. Soc.*, 2007, **154**, D697.
46 A. Niaz, J. Fischer, J. Barek, B. Yosypchuk, Sirajuddin and M. I. Bhanger, *Electroanalysis*, 2009, **21**, 1786–1791.
47 G. Rounaghi, R. M. Kakhki and H. Azizi-Toupkanloo, *Mater. Sci. Eng., C*, 2012, **32**, 172–177.
48 X. X. Jiao, H. Q. Luo and N. B. Li, *J. Electroanal. Chem.*, 2013, **691**, 83–89.
49 G. Kenne Dedzo, E. Pameté Yambou, M. R. Topet Saheu, G. Ngnie, C. P. Nanseu-Njiki, C. Detellier and E. Ngameni, *J. Electroanal. Chem.*, 2017, **801**, 49–56.
50 Y. Zhang, L. Wu, W. Lei, X. Xia, M. Xia and Q. Hao, *Electrochim. Acta*, 2014, **146**, 568–576.
51 C. Zhang, S. Govindaraju, K. Giribabu, Y. S. Huh and K. Yun, *Sens. Actuators, B*, 2017, **252**, 616–623.